ISSN (Print) 1226-1750
ISSN (Online) 2233-6656
Journal of Magnetics 31(2), 178-186 (2026) https://doi.org/10.4283/JMAG.2026.31.2.178

Inverse Reconstruction and Degradation Modeling of Local Magnetic Properties Near Cutting Edge

Yuan Liu[1], Shuaichao Yue[1,2]*, Yongjian Li[1], Jiatong Yin[1], Baoliang Zhao[1], and Hongtao Shi[1]

[1]*State Key Laboratory of Intelligent Power Distribution Equipment and System, Hebei University of Technology, Tianjin 300401, China*
[2]*Hubei Provincial Engineering Technology Research Center for Power Transmission Line, China Three Gorges University, Yichang 443002, China*

(Received 28 February 2026, Received in final form 21 May 2026, Accepted 22 May 2026)

The needle probe method for local magnetic property measurements involves a trade-off between spatial resolution and measurement accuracy. A larger probe spacing limits local resolution, whereas a smaller spacing produces significant errors. This study proposes an inverse method to reconstruct the localized magnetic flux density at smaller step sizes from measurements using a relatively large probe spacing. Moreover, a degradation model is developed based on the reconstructed and measured data, describing the reduction in the magnetic flux density and increase in the magnetic loss as a function of the distance from the edge and applied magnetic field. Experimental results demonstrate that the prediction errors of the model are less than 3 %.

Keywords : local magnetic properties, needle probe method, inverse method, degradation model

1. Introduction

Non-oriented electrical steel, with its excellent magnetic properties, is widely used in electrical equipment such as electric motors and generators. During manufacturing of electrical machine cores, steel sheets are typically subjected to various processes, including stamping, bending, cutting, stacking, and welding; among these processes, cutting has the most significant effect on magnetic properties [1–3]. Therefore, precise characterization of local magnetic properties near the cut edge and modeling that accounts for the degraded region are crucial for accurate design of electrical devices.

To achieve nondestructive measurements of magnetic properties at the cut edge, needle probe methods are commonly employed to capture local magnetic flux density. The working principle of probe-based measurements involves calculating the voltage between two points on the sample surface, where the measured voltage is proportional to the rate of change in the magnetic flux density between the probe tips within the sample. K. Senda *et al.* measured the edge magnetic properties of silicon steel using a 10 mm probe and Hall sensor [4]. Li *et al.* employed 2-mm spaced *B*-probes and single-layer *H*-coils to study magnetic properties at the cut edges of laser-cut and wire-cut non-oriented electrical steel [5]. N. J. Lewis and team combined 2.5-mm spaced *B*-probes with Hall sensors to construct a movable integrated *B–H* sensor for measuring the local magnetic properties of non-oriented steel, identifying a degradation width of approximately 3 mm caused by stamping [6].

Measurements of local magnetic properties using this method are subjected to several constraints: (1) the magnetic flux distribution inside samples is symmetric with respect to the axis parallel to the surface where the probes are placed, (2) the minimum distance between the probe tips and edge is not less than half the sample thickness [7], and (3) the probe spacing is relatively large compared with the sample thickness, allowing the thickness to be neglected [8, 9]. Constraint (1) can be satisfied by applying symmetric excitation to samples, and constraint (2) may result in measurement blind zones, where the most severe degradation occurs, while constraint (3) reduces the ability to characterize local properties. Therefore, improving the local characterization capability of data within acceptable measurement errors is critical.

In this study, an integrated *B–H* sensor comprising probes and TMR elements is used to measure local magnetic properties within 10 mm of the edge of laser-cut

©The Korean Magnetics Society. All rights reserved.
*Corresponding author: Tel: +86 15222035571
e-mail: yues22@hebut.edu.cn

non-oriented silicon steel. Based on the probe spacing and probe movement step size, an inverse method is proposed to reconstruct the localized magnetic flux density over smaller regions using estimates obtained with a relatively large probe spacing. This method formulates a discrete inverse problem, enabling reconstruction of local magnetic properties from finite-window integral measurements and validating the characterization capability of a 2 mm probe. Then, a dual-valued continuous degradation model is established, which incorporates the magnetization curves depending on the distance from the cut edge x and magnetic field strength H as well as the magnetic loss curves dependent on the x and magnetic flux density B. The model predicts local magnetic properties with maximum errors below 3 % (H > 50 A/m) and 2.3 % (B > 0.4 T). The proposed methods and models provide a novel approach for refined modeling and accurate design of electrical devices.

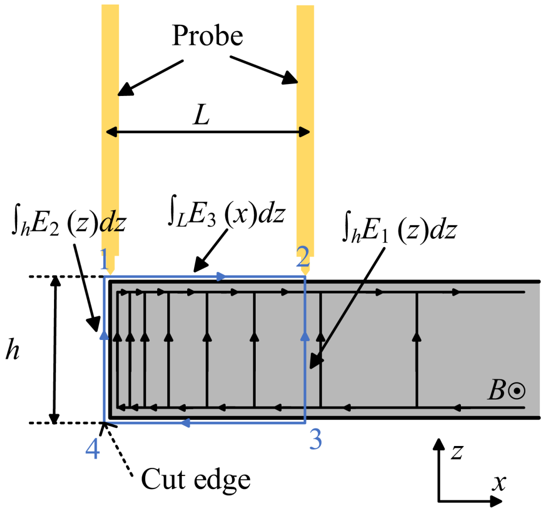

Fig. 1. (Color online) Eddy current paths (black lines) and integration path (blue line).

2. Measurement Setup and Results

2.1. Needle Probe Method and Error Analysis

The needle probe method is based on Faraday's law of electromagnetic induction. Assuming that the magnetic flux density has only a Y component, the induced current density contains only X and Z components. As shown in Fig. 1, voltages V_{12} and V_{34} depend solely on the X component of the electric field, while voltages between points V_{14} and V_{23} depend on the Z component. Because V_{14} and V_{23} cannot be directly measured, they are typically assumed to be zero or negligible compared with V_{12} and V_{34}; thus, (1) is reduced to (2).

$$\begin{cases} V_{12} = V_{34} = U_{B\text{probe}} = \int_L E_3(x)dx \\ V_{41} = \int_h E_2(z)dz \quad V_{23} = -\int_h E_1(z)dz \\ \int_h E_2(z)dz + 2\int_L E_3(x)dx - \int_h E_1(z)dz = -\int_S \frac{\partial B(y)}{\partial t} \cdot dS \end{cases} \tag{1}$$

$$V_{12} = \int_L E_3(x)dx = -\frac{1}{2}\int_S \frac{\partial B(y)}{\partial t} \cdot dS \tag{2}$$

where h is the sheet thickness, L is the probe spacing, and S is the surface enclosed by the rectangular loop 1234. $U_{B\text{probe}}$ denotes the probe voltage. E_1 and E_2 are the vertically induced electric fields, and E_3 is the induced electric field along the probe spacing.

For edge-region measurements, where the probes must be placed close to the cut edge, constraint (2) triggers, introducing a nonnegligible error. This error was analyzed in [10]. When the probe tips are aligned with the cut edge, the induced electric fields between points 1–4 and 2–3 satisfy Eq. (3). The resulting error D arising from neglecting the vertical component of the induced electromotive force is given by Eq. (4).

$$\int_h E_1(z)dz = \int_h E_2(z)dz e^{-6L} \tag{3}$$

$$D = \frac{-\int_S \frac{\partial B(y)}{\partial t} \cdot dS - 2U_{B\text{probe}}}{-\int_S \frac{\partial B(y)}{\partial t} \cdot dS} \tag{4}$$

Fig. 2 illustrates the distributions of the x and z components of the induced electric field intensity near the cut edge of a specimen. By substituting the data in Fig. 2 into Eqs. (1)–(4), the error is calculated to be 4.92 % for a probe spacing of 2 mm and a sample thickness of 0.5 mm. Because the actual sample thickness in this study is 0.35 mm, the corresponding error is expected to be smaller.

To evaluate the error induced by constraint (3) as a function of the probe spacing, the peak local magnetic flux density at 50 Hz was measured in the unaffected central region (>15 mm from the cut edge). Measurements at a probe spacing of 18 mm were used as the reference. Fig. 3 shows the relative error of the peak local magnetic flux density versus probe spacing at overall magnetic flux densities of 0.8, 1.0, and 1.5 T. The relative error decreases with increasing probe spacing and slightly decreases with increasing magnetic flux density. For all probe spacings, the error remains below 3 %.

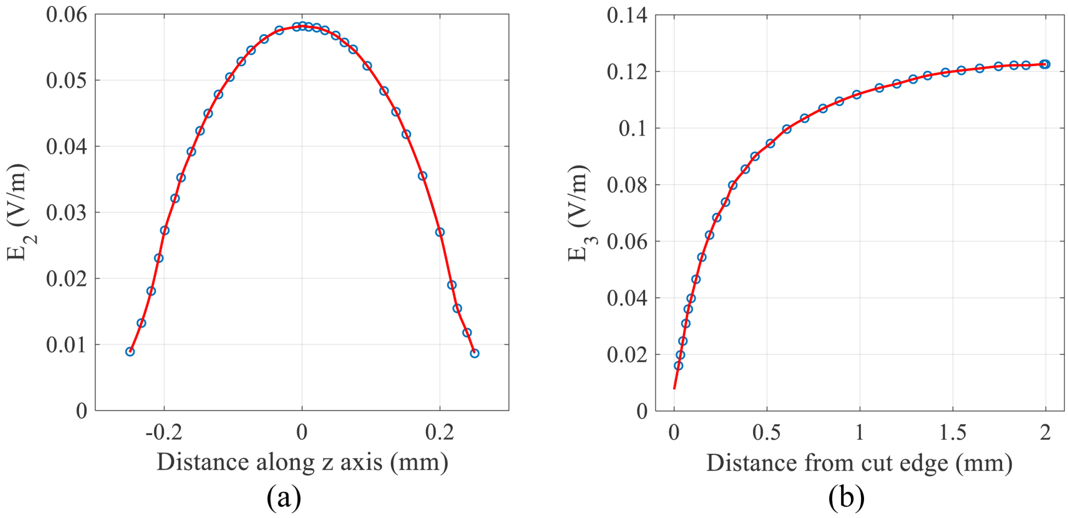

Fig. 2. (Color online) Calculated distribution of the local values of the electric field intensity components: $E_2(z)$ (a) and $E_3(x)$ (b).

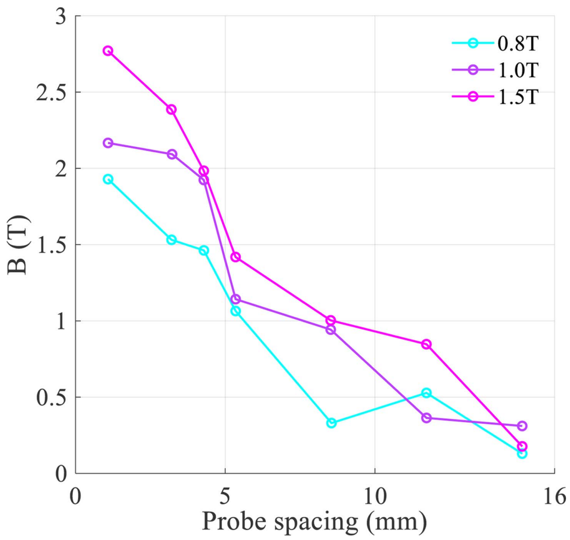

Fig. 3. (Color online) Relative errors in magnetic flux density measurements for probes with different spacings.

In addition, the error caused by the air magnetic flux is negligible. For instance, when the local magnetic flux density is 1.5 T, the corresponding magnetic field strength is 950 A/m. According to the continuity condition of the magnetic field strength at the interface, the corresponding air flux density is approximately 0.0012 T, resulting in a relative error of only 0.08 %.

The integrated *B–H* sensor consisted of two opposing TMR elements and a *B* probe with a 2 mm spacing between them. The TMR outputs were connected in a differential configuration to enhance noise resistance, and the probe tip could retract to ensure close contact with the sample surface, as shown in Fig. 4(a).

During measurements, the specimen was placed in a single-sheet tester (SST), with two series-connected 15-turn global *B*-coils wound around it to maintain a sinusoidal magnetic flux density inside the sample. The

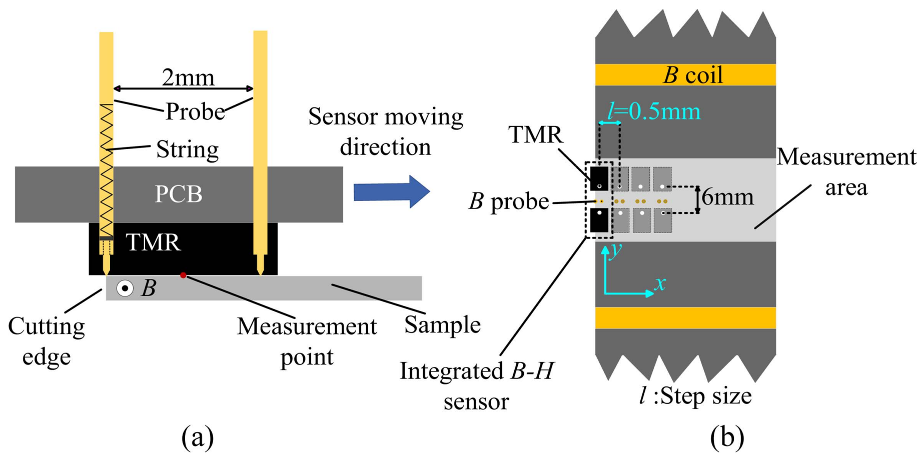

Fig. 4. (Color online) Front view (a) and top view (b) of integrated *B–H* sensor movement.

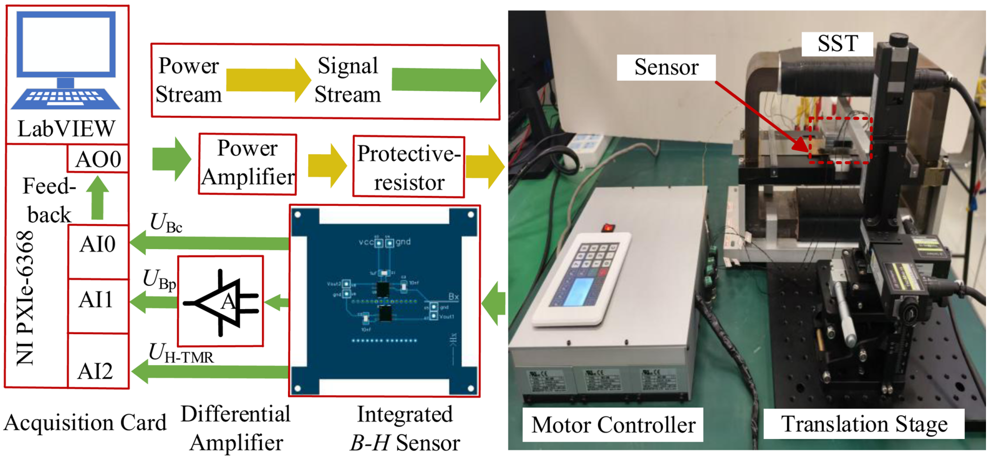

Fig. 5. (Color online) Schematic of the magnetic measurement system for the edge degradation region.

integrated *B–H* sensor was mounted on a three-axis translation stage to measure magnetic properties at different positions near the cutting edge, as shown in Fig. 4(b). Fig. 5 shows a schematic of the localized magnetic property measurement system. In addition, to show that the sample and setup geometry do not affect the results, finite-element simulations of the undegraded sample were conducted. Fig. 6(a) shows the 3D model, in which magnetic properties are adopted from the central region of the actual sample (>15 mm from the edge). Fig. 6(b) presents the magnetic flux density along the center line. The results indicate that the magnetic flux density is uniform and independent of the distance from the cut edge for the undegraded sample.

2.2. Measurement result

The measurement setup was used to characterize the alternating magnetic properties of laser-cut non-oriented silicon steel. Measurements were performed on the specimen surface at $y = 0$ over a range from $x = 1$ mm to 8 mm, with a step size of 0.5 mm, yielding 15 points.

Fig. 7 illustrates the variation in the local magnetic flux density and its relative increment from the central region as a function of the distance from the cutting edge. The magnetic flux density increases monotonically from the cutting edge toward the specimen center, and the magnetic degradation effect gradually weakens with increasing magnetic flux density. For example, when the magnetic flux density at 5.5 mm reaches 1.0 T, the value at 1 mm from the edge is only 0.63 T, corresponding to a reduction of 37 %; this reduction falls to 12 % at 1.4 T. Beyond a distance of 5.5 mm, the magnetic flux density remains nearly constant.

Fig. 8 shows the magnetic loss and its relative increment

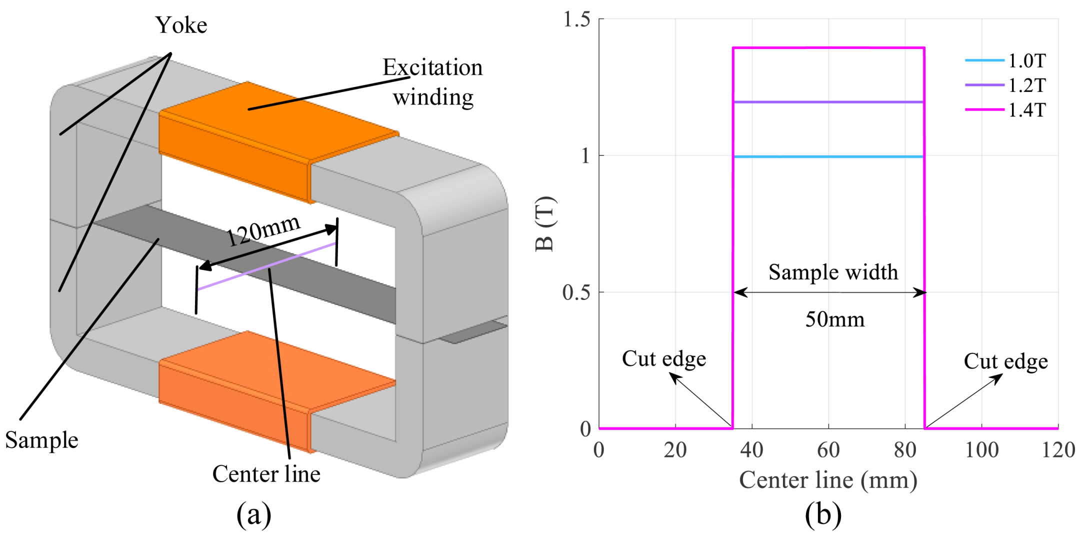

Fig. 6. (Color online) Finite-element model (a) and magnetic flux density distribution along the center line (b).

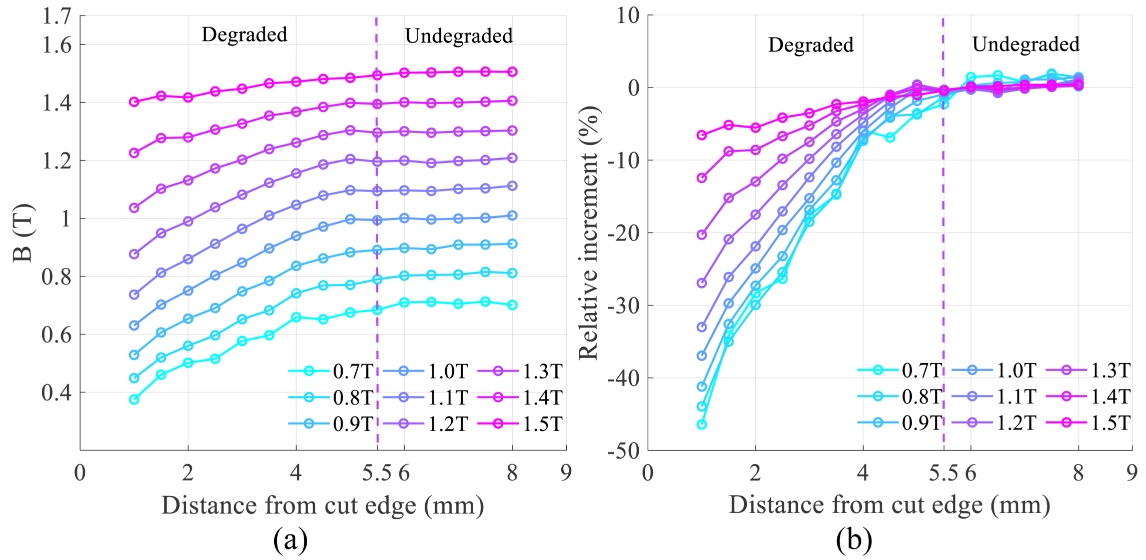

Fig. 7. (Color online) Variation in the peak magnetic flux density (a) and its relative increment with the distance (b).

with the distance from the cut edge. As the distance increases, the magnetic loss gradually decreases, with a sharper decline observed in the high-magnetic-flux-density region (>1 T). At 1.0 T, the loss decreases from 0.99 W/kg at 5.5 mm to 0.86 W/kg at 1 mm, corresponding to a reduction of 15 %. This reduction increases to 43 % at 1.4 T, showing a trend opposite to that observed in Fig. 7(b). Beyond 5.5 mm, the magnetic loss stabilizes.

3. Inverse Method and Degradation Model

Based on the measurement data presented in Section 2.2, an inverse method that reduces the effective averaging range of the magnetic flux density without relying on a small probe spacing is proposed. Using this inverse method, the averaged magnetic flux density over a 1 mm range is obtained and compared with that obtained using a 2 mm probe to validate the local representativeness of the 2 mm probe. Furthermore, a bivariate degradation model that does not depend on any predefined functional form is established based on the measured data.

3.1. Inverse method

The proposed inverse approach formulates a discrete inverse problem that enables the effective averaging range of the measured magnetic flux density to be reduced

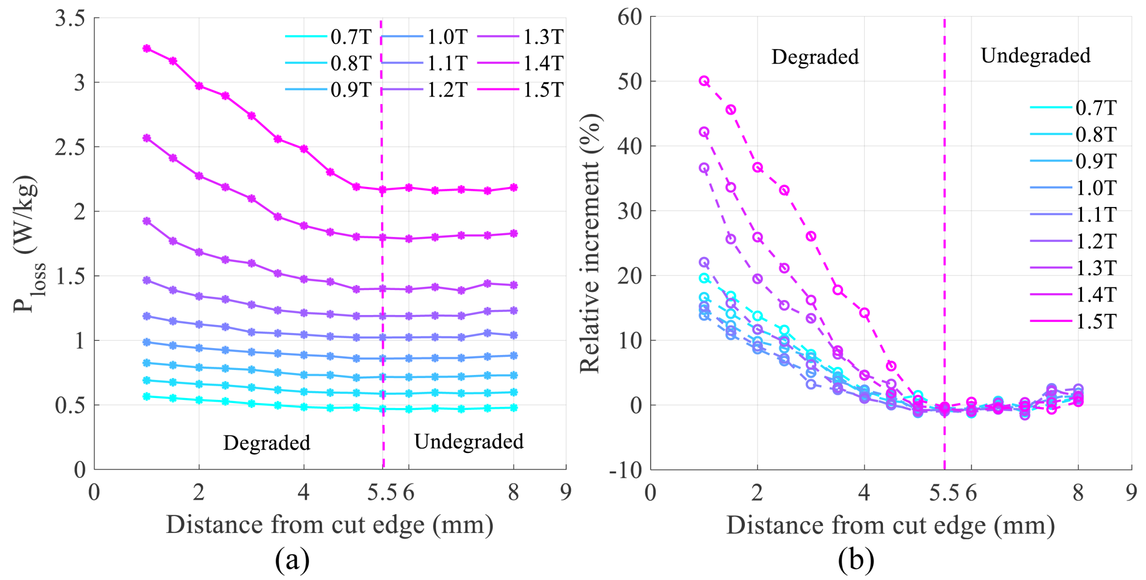

Fig. 8. (Color online) Variation in the loss (a) and its relative increment (b) with the distance.

without physically decreasing the probe spacing. This method makes the following assumptions:

(1) The magnetic flux density is constant in the undegraded region, as shown in Fig. 7.

(2) The probe-measured averages follow Eq. (5).

(3) The probe spacing is an integer multiple of the sensor step size, which is ensured by the translation stage.

$$B_{a+L/2} = \frac{1}{L}\int_{a}^{a+L} B(H,x)\,dx \tag{5}$$

where $B(H, x)$ is the actual magnetic flux density at distance x, a denotes the minimum distance from the probe tip to the edge, L is the probe spacing, and $B_{a+L/2}$ is the probe-measured average magnetic flux density over L.

Initially, the degradation depth δ is inferred from the experimental data. With a probe spacing of 2 mm and a step size of 0.5 mm, the measured magnetic flux density at 5 mm represents the average value over 4–6 mm, while that at 5.5 mm corresponds to the average value over 4.5–6.5 mm. As shown in Fig. 9, the difference between these measurements corresponds to S_a–S_b, while subtracting the 5.5 mm reading from the 6 mm reading yields S_d–S_c. Because the magnetic flux density values remain constant beyond 5.5 mm, the following order is observed: $S_g < S_b < S_c = S_e = S_f = S_a = S_d$, indicating that the actual degradation depth (δ) lies within 4.5–5 mm.

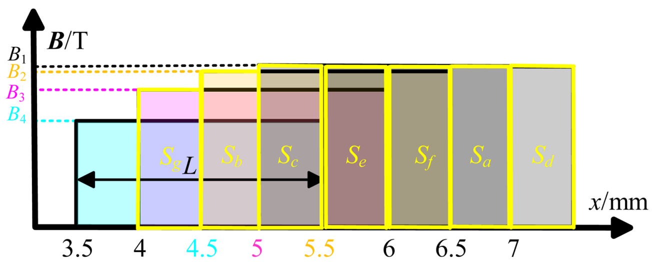

Fig. 9. (Color online) Schematic diagram for determining the degradation depth.

$$\begin{aligned}
L(B_{3l}\text{-}B_{2l}) &= S_5\text{-}S_1 & L(B_{8l}\text{-}B_{7l}) &= S_{10}\text{-}S_6\\
L(B_{4l}\text{-}B_{3l}) &= S_6\text{-}S_2 & L(B_{9l}\text{-}B_{8l}) &= S_{11}\text{-}S_7\\
L(B_{5l}\text{-}B_{4l}) &= S_7\text{-}S_3 & L(B_{10l}\text{-}B_{9l}) &= S_{12}\text{-}S_8\\
L(B_{6l}\text{-}B_{5l}) &= S_8\text{-}S_4 & L(B_{11l}\text{-}B_{10l}) &= S_{13}\text{-}S_9\\
L(B_{7l}\text{-}B_{6l}) &= S_9\text{-}S_5 & L(B_{12l}\text{-}B_{11l}) &= S_{14}\text{-}S_{10}
\end{aligned} \tag{6}$$

$$L(B_{13l}\text{-}B_{12l}) = S_{15}\text{-}S_{11} = 0 \tag{7}$$

Assuming that $B(H, x)$ varies with the distance from the cut edge, as shown in Fig. 10, where $L = 4l = 2$ mm and

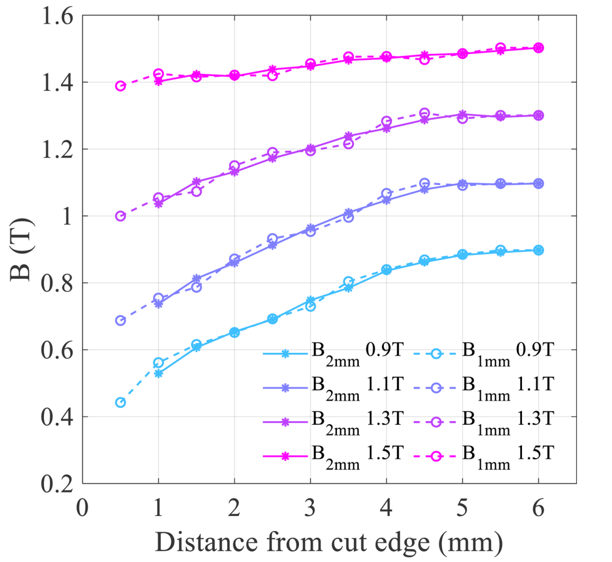

Fig. 11. (Color online) Comparison of 1 mm averages with 2 mm measurements.

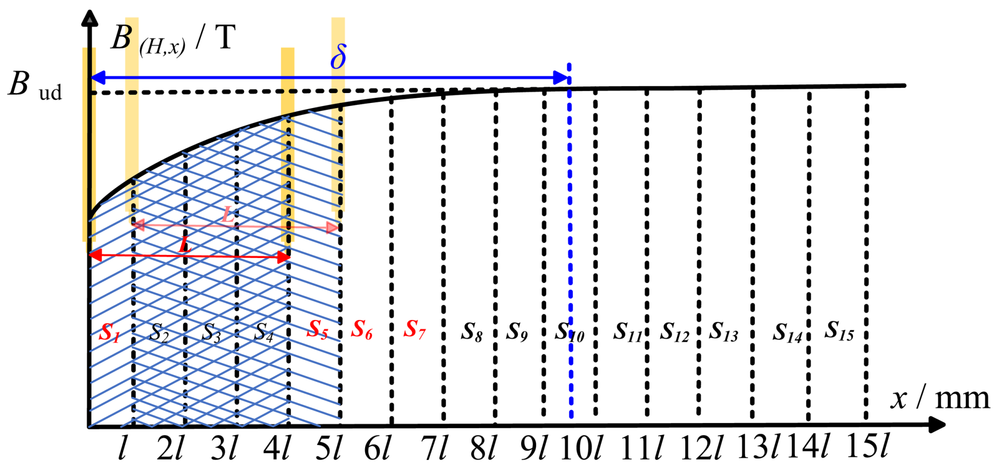

Fig. 10. (Color online) Schematic diagram of the inverse method.

$9l < \delta < 10l$ (where l is the step size), the differences between the data measured at consecutive step distances are calculated. Applying Eq. (5) to these differences yields Eqs. (6) and (7).

The sum of S_i and S_{i+1} reconstructs the 1 mm averaged magnetic flux density, which is compared with that obtained at a 2 mm probe spacing. As shown in Fig. 11, the reconstructed results closely match the 2 mm data, indicating that the 2 mm average probe spacing effectively represents the midpoint between the probe tips. The inverse method can be expressed in a unified form, given by Eqs. (8)–(12).

$$B_{(k+1)l+\frac{L}{2}} - B_{kl+\frac{L}{2}} = \begin{cases} \frac{1}{L}\left(S_{1+k+\frac{L}{l}} - S_{1+k}\right) & k=0,1,2,......,N-1 \quad L \ge \delta \\ \frac{1}{L}\begin{cases} S_{1+\frac{L}{l}} - S_1 & k=0 \\ \vdots & \vdots \\ S_{N+k+1-\frac{L}{l}} - S_{N+k+1-2\frac{L}{l}} & k=1,2,\cdots,\frac{L}{l} \\ S_{N+k+1} - S_{N+k+1-\frac{L}{l}} & k=1,2,\cdots,\frac{L}{l} \end{cases} & L<\delta \end{cases} \tag{8}$$

$$S_{i \ge N+1} = lB_{\mathrm{ud}} \tag{9}$$

$$N = k_0 \qquad \left(B_{(k_0+1)l+\frac{L}{2}} - B_{k_0 l+\frac{L}{2}} = 0\right) \tag{10}$$

$$B_{(k_0+1)l+\frac{L}{2}} = B_{k_0 l+\frac{L}{2}} = B_{\mathrm{ud}} \tag{11}$$

$$(N-1)l \le d \le Nl \tag{12}$$

3.2. Degradation model

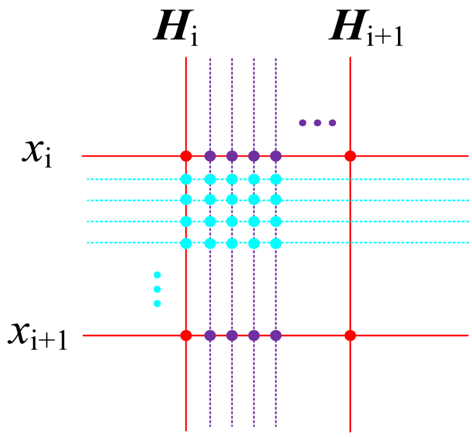

Fig. 12. (Color online) Schematic of the refined mesh for $y(H, x)$.

The degradation model characterizes the reduction in the magnetic flux density and increase in the magnetic loss as a function of the distance from the edge and applied magnetic field strength or magnetic flux density. Based on the magnetization and loss curves measured at various distances from the cutting edge, the continuous spatial decay functions are obtained. The detailed derivation steps of the model are as follows.

Fig. 7 shows the peak magnetic flux density drop at the cutting edge. To model edge magnetization, the magnetic flux reduction $\Delta B(H, x)$ is assumed to depend on the distance x and field H. At $x = 0$, $\Delta B_{\max}(H)$ is observed, and $\Delta B(H) = 0$ for $x \ge \delta$. The spatial distribution of the magnetic flux density reduction is given by the following equation:

$$\Delta B(H,x) = \Delta B(H)_{\max} \cdot y(H,x) \tag{13}$$

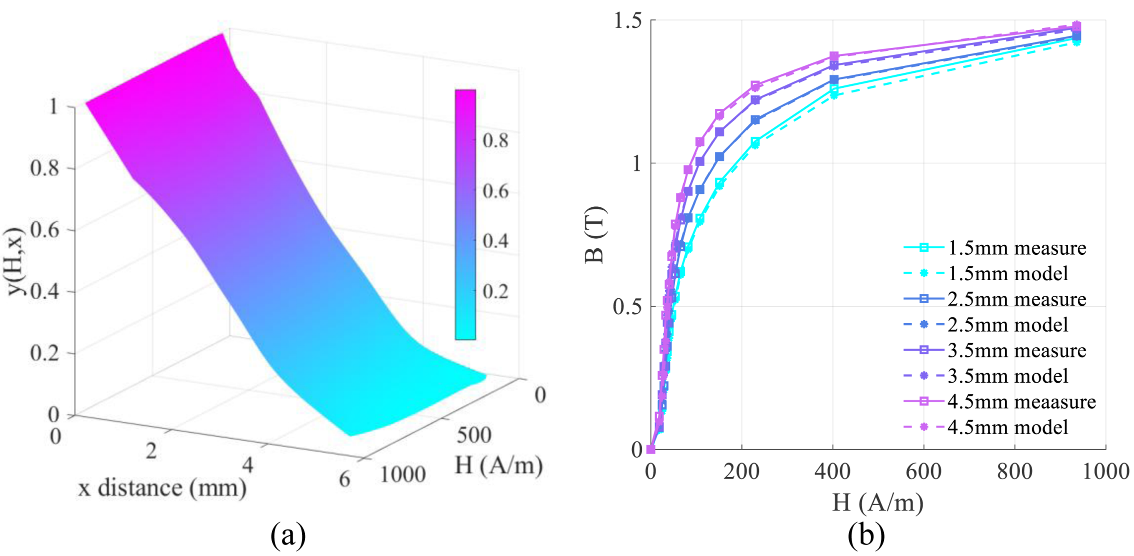

Fig. 13. (Color online) $y(H, x)$ (a) and magnetization model validation (b).

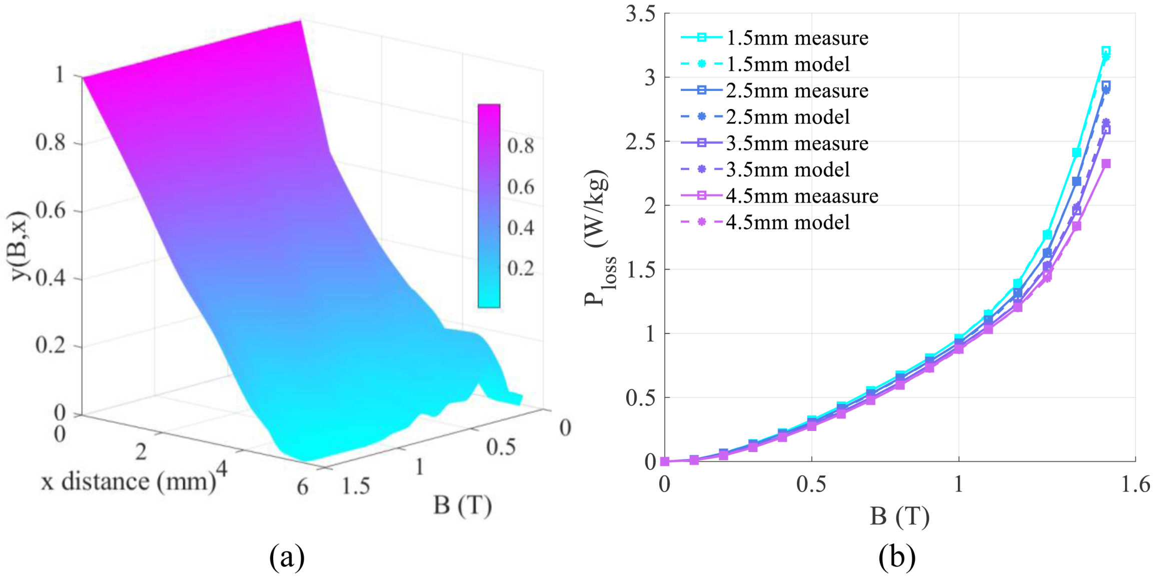

Fig. 14. (Color online) $y(B, x)$ (a) and loss model validation (b).

Therefore, the spatial distribution of the measured average magnetic flux density can be expressed as follows:

$$B(H,x) = B(H,x>\delta) - \Delta B(H)_{\max} \cdot y(H,x) \tag{14}$$

$$\Delta B(H)_{\max} = B(H,x>\delta) - B(H,x=0) \tag{15}$$

In Eq. (15), $B(H, x = 0)$ is obtained by exponential extrapolation of the reconstructed data at $x = 1$, 2 and 3 mm derived from the inverse method, thereby yielding $\Delta B(H)_{\max}$. The original H_i–x_i mesh is too coarse; Fig. 12 shows the process of refining it. Hermite interpolation is applied to refine the H_i–x_i mesh and smooth $y(H, x)$.

The magnetization curves measured at 1, 2, 3, 4, 5 and 5.5 mm from the edge are used in the model to identify $y(H, x)$, while those measured at 1.5–4.5 mm are used to validate the accuracy of the model. Fig. 13(a) shows that the identified function $y(H, x)$ decreases with increasing x from 1 at the edge to 0 at 5 mm and slightly with increasing H. Fig. 13(b) compares the measured and predicted magnetization curves. For $H > 50$ A/m, errors remain below 3%, confirming the accuracy of the model.

Similarly, a maximum increase in the magnetic loss is assumed at the cutting edge. Accordingly, Eqs. (12)–(14) are transformed into Eqs. (16)–(18) to establish a magnetic loss model near the edge, with the function to be identified denoted as $y(B, x)$.

$$\Delta P(B,x) = \Delta P(B)_{\max} \cdot y(B,x) \tag{16}$$

$$P(B,x) = P(B,x>\delta) + \Delta P(B)_{\max} \cdot y(B,x) \tag{17}$$

$$\Delta P(B)_{\max} = P(B,x=0) - P(B,x>\delta) \tag{18}$$

In Eq. (18), $P(B, x = 0)$ is obtained by exponential extrapolation of the data at $x = 1$, 2 and 3 mm to derive $\Delta P(B)_{\max}$. The magnetic loss curves at 1, 2, 3, 4, 5 and 5.5 mm from the edge are used to identify $y(B, x)$. Fig. 14(a) shows $y(B, x)$, and Fig. 14(b) compares the measured and predicted loss curves at 1.5–4.5 mm, demonstrating strong agreement. For $B > 0.4$ T, the maximum prediction error is 2.3 %.

4. Conclusion

This study proposes an inverse method to derive the localized magnetic flux density over a reduced step size from measurements acquired at a relatively large probe spacing. Using this method, the magnetic properties of the 10 mm area around the edge of the silicon steel sheet are reconstructed and analyzed at a step size of 0.5 mm. A degradation model that describes the reduction in the magnetic flux density and increase in the magnetic loss as a function of the distance from the edge and applied magnetic field or magnetic flux density is then established. The decay functions are identified from both the measured and reconstructed data, and experimental validation reveals that the prediction errors are less than 3%. This study provides an effective approach for local magnetic property measurement and refined modeling of electrical devices.

Acknowledgment

This work was supported by the National Natural

Science Foundation of China (Grant Nos. 52130710 and 52407005) and by Hubei Provincial Engineering Technology Research Center for Power Transmission Line, China Three Gorges University (Grant No. 2024KXL04).

References

[1] J. Gao, S. Yue, Y. Dou, J. Zhou, J. Yin, and Y. Li, IEEE Trans. Instrum. Meas. **74**, 6000408 (2025).
[2] Z. Gmyrek, IEEE Trans. Instrum. Meas. **7**, 1661 (2016).
[3] A. Schoppa, J. Schneider, and C.-D. Wuppermann, J. Magn. Magn. Mater. **2**, 74 (2000).
[4] K. Senda, M. Kurosawa, M. Ishida, M. Komatsubara, and T. Yamaguchi, J. Magn. Magn. Mater. **2**, 136 (2000).
[5] Y. Li, Y. Fu, Y. Dou, C. Zhang, and K. Zhang, AIP Advances. **2**, 025115 (2021).
[6] N. J. Lewis, P. I. Anderson, Y. Gao, and F. Robinson, J. Magn. Magn. Mater. **15**, 495 (2018).
[7] H. Pfutzner and G. Krismanic, IEEE Trans. Magn. **3**, 1610 (2004).
[8] T. Yamaguchi, K. Senda, M. Ishida, K. Sato, A. Honda, and T. Yamamoto, J. Phys. Iv. **8**, PR2_717 (1998).
[9] M. De Wulf, L. Dupré, D. Makaveev, and J. Melkebeek, J. Appl. Phys. **10**, 8271 (2003).
[10] Z. Gmyrek, J. Magn. Magn. Mater. **1**, 9 (2016).